

Two-photon absorption of FAPbBr₃ perovskite nanocrystals

Xuanyu Zhang(张轩宇)¹, Shuyu Xiao(肖书宇)², Xiongbin Wang(王雄彬)¹, Tingchao He(贺廷超)², and Rui Chen(陈锐)^{1,†}

¹Department of Electrical and Electronic Engineering, Southern University of Science and Technology, Shenzhen 518055, China

²College of Physics and Optoelectronic Engineering, Shenzhen University, Shenzhen 518060, China

(Received 12 December 2022; revised manuscript received 7 January 2023; accepted manuscript online 11 January 2023)

Perovskite nanocrystals (NCs) with high two-photon absorption (TPA) cross-section are of great interest due to their potential applications in three-dimensional optical data storage and multiphoton fluorescence microscopy. Among various perovskite materials, FAPbBr₃ NCs show a better development prospect due to their excellent stability. However, there are few reports on their nonlinear optical properties. In this work, the nonlinear optical behavior of FAPbBr₃ NCs is studied. The methods of multiphoton absorption photoluminescence saturation and open aperture Z-scan technique were applied to determine the TPA cross-section of FAPbBr₃ NCs, which was around $2.76 \times 10^{-45} \text{ cm}^4 \cdot \text{s} \cdot \text{photon}^{-1}$ at 800 nm. In addition, temperature-dependent photoluminescence induced by TPA was investigated, and the small longitudinal optical phonon energy and electron-phonon coupling strength was obtained, which confirm the weak Pb-Br interaction. Meanwhile, it is found that the exciton binding energy in FAPbBr₃ NCs was 69.668 meV, which may be ascribed to the strong hydrogen bond interaction. It is expected that our findings will promote the application of FAPbBr₃ NCs in optoelectronic devices.

Keywords: FAPbBr₃ nanocrystals, two-photon absorption cross-section, Z-scan, multiphoton absorption photoluminescence saturation

PACS: 42.65.-k, 42.62.Fi, 42.70.Nq

DOI: 10.1088/1674-1056/acb203

1. Introduction

Two-photon absorption (TPA) is an interesting optical phenomenon with promising applications, even though the experiments have been observed for about 60 years. Due to the small excitation photon energy, the TPA-induced emission possesses enormous advantages over traditional luminescence. For instance, it reduces the risk of phototoxicity for biological molecules,^[1-3] compared with single photon excitation. Moreover, the TPA can only take place on the focal plane, which results in imaging with high spatial resolution.^[4-6] Benefiting from these advantages, materials with high TPA cross-section (σ_2) are of great potential in ultrafast lasers, optical data storage, and medical imaging.^[7-10] In order to develop and apply these techniques, it is necessary to fully understand the physical processes behind TPA activities of the materials and determine the precise values. To date, a large number of materials have been reported for TPA application. Experimental results have shown that perovskites have better nonlinear optical (NLO) properties because of their large TPA cross-section, compared with traditional CdSe, CdTe semiconductors, and well-designed organic molecules.^[11-16]

In recent years, there has been an explosive growth in the reports of TPA cross-sections of various perovskite nanomaterials, including quantum dots (QDs), nanorods (NRs), nanoplatelets (NPLs), and nanocrystals (NCs) under different excitation wavelengths from 700 nm to 1100 nm. Moreover, for perovskite nanomaterials with different sizes and composi-

tions at different wavelengths, the value varies greatly, which may exceed two orders of magnitude. For example, Pullerits *et al.* presented the measurement of size- and wavelength-dependent TPA cross-section of perovskite QDs.^[15] It is reported that the TPA cross-section of perovskite QDs shows a power-law size dependence $\sigma_2 \propto d^{3.3}$, and follows the one-photon linear absorption cross-section σ_1 wavelength dependence. To be more specific, Sum *et al.* reported that giant TPA properties for core-shell MAPbBr₃/(OA)₂PbBr₄ NCs with $\sigma_2 \sim 5.0 \times 10^6 \text{ GM}$ (1 GM = $10^{-50} \text{ cm}^4 \cdot \text{s} \cdot \text{photon}^{-1}$) at 800 nm,^[17] while the value of CsPbBr₃ reported by Samoć and co-workers just around $1.6 \times 10^4 \text{ GM}$ at 675 nm.^[18] Although the NLO of many different perovskite materials have been reported, for FAPbBr₃ perovskite, no matter what morphology and composition, only a few articles have observed the nonlinear optical phenomena,^[19,20] while detailed analysis of NLO activity has not been reported. This research gap is regrettable, because FAPbBr₃ possesses better thermal stability and excellent carrier transport characteristics than traditional MAPbBr₃, which has great potential in device applications.^[21,22]

Therefore, in this work, the TPA cross-section of FAPbBr₃ NCs was determined to be about $2.76 \times 10^{-45} \text{ cm}^4 \cdot \text{s} \cdot \text{photon}^{-1}$ at 800 nm by the multiphoton absorption photoluminescence saturation (MPAPS) and open aperture (OA) Z-scan technique. In addition, the emission induced by TPA was studied by temperature-dependent photoluminescence (PL) spectroscopy. By fitting the photon energy, full wavelength at half maximum (FWHM), and the integrated

[†]Corresponding author. E-mail: chenr@sustech.edu.cn

PL intensity, these following physical parameters have been derived: the temperature coefficient is $0.360 \text{ meV}\cdot\text{K}^{-1}$, the longitudinal optical (LO) phonon energy is 16.900 meV , the electron–phonon (EP) coupling strength is 44.464 meV , and the exciton binding energy is 69.668 meV . The smaller EP coupling strength and LO phonon energy confirm the inhibition of Pb–Br interaction, which leads to the weaker NLO behavior of FAPbBr₃ NCs.

2. Experimental details

2.1. Synthesis of FAPbBr₃ NCs

All reagents were purchased and used without further purification, including FA-acetate (Sigma-Aldrich), Pb(CH₃COO)₂ × 3H₂O (Sinopharm Chemical Reagent Co., Ltd., ≥ 99.5%), octadecene (ODE, Sigma-Aldrich, 90%), OA (Sigma-Aldrich, 90%), OAmBr (Xi'an Polymer Light Technology Crop), and toluene (Sinopharm Chemical Reagent Co., Ltd., ≥ 99.5%). Briefly, FA-acetate (0.078 g, 0.75 mmol), Pb(CH₃COO)₂ × 3H₂O (0.076 g, 0.2 mmol), OA (2 mL, vacuum dried at 120 °C), and ODE (8 mL, vacuum-dried at 120 °C) were loaded into a 100-mL flask and dried for 30 min under vacuum at 50 °C. The mixture was heated to 130 °C under N₂ atmosphere and OAmBr (0.21 g, 0.6 mmol) in toluene (2 mL) was injected. After 10 s, the reaction mixture was cooled on an ice–water bath. The green solution of FAPbBr₃ NCs was collected, and stored at 4 °C. Then, the nanocrystalline concentration of the solution is characterized by an inductively coupled plasma mass spectrometer (ICP-MS, Agilent 7700X).

2.2. Structural characterization

Transmission electron microscopy (TEM) measurements were prepared through dropping a relatively dilute solution of colloidal NCs onto carbon-coated 200 mesh copper grids. Conventional TEM images were acquired by an FEI Talos F200X microscope equipped with a thermionic gun under acceleration voltage of 200 kV. The current of the 1-nm electron beam at this voltage is 1.5 nA, and the resolution is 0.12 nm. X-ray diffraction (XRD) measurements were recorded on a Bruker D8 Discover system.

2.3. Optical characterization

The linear absorption spectra were recorded on an ultraviolet-visible (UV-vis) spectrophotometer (Lambda 950, PerkinElmer, Inc.) at room temperature. All the samples were excited by femtosecond laser pulses (Coherent Astrella ultrafast Ti:sapphire laser with OperA Solo, pulse width of 100 fs and repetition rate of 1 kHz). The PL signals were dispersed by monochromator (Andor SR-750-D1-R), and detected using a Newton charge-coupled device (model No. DU920P-BU).

The NCs were drop-casted on the a quartz substrate with a size of $1 \text{ cm} \times 1 \text{ cm} \times 1 \text{ mm}$, and placed inside a closed-cycle helium cryostat with quartz windows for temperature-dependent PL measurements. The temperature is well-controlled from 80 K to 300 K. During the OA Z-scan measurements, femtosecond pulses at 800 nm were focused on the samples by a lens with a focal length of 500 mm, and the transmitted light was then measured by a silicon detector.

3. Result and discussion

Figure 1(a) shows the typical TEM image of FAPbBr₃ NCs. The sample is cubic in shape with good dispersion, which confirms the successful synthesis of NCs. According to statistics, the average diameter of FAPbBr₃ NCs is $10.0 \pm 0.1 \text{ nm}$. Figure 1(b) presents the XRD patterns of the NCs, where the diffraction peaks can be indexed to the lattice planes of cubic perovskite crystal structures.^[23] No diffraction peak from impurity phase can be detected. The normalized UV-vis absorption and PL emission spectra of FAPbBr₃ NCs were plotted in Fig. 1(c). It can be seen that the FAPbBr₃ NCs show a continuous broad absorption in the range of 2.20 eV–2.55 eV with obvious shoulder at 2.41 eV, which is consistent with the previous reports.^[22,24–26] A symmetrical emission at 2.30 eV with an FWHM of 90.9 meV has been observed under the excitation of 3.10 eV. When the excitation energy is reduced to 1.55 eV, the normalized PL spectrum fully overlaps with the spectrum in Fig. 1(c), which indicates that the FAPbBr₃ NCs are two-photon active materials.

Figure 2(a) shows the power dependent PL spectra in the range of 0.1 mW–90.0 mW. It is obviously that the integrated PL intensity initially increases with the excitation power. The quadratic relationship between PL intensity and excitation power at lower power (0.10 mW–20.00 mW) is displayed in Fig. 2(b). The linear fitting with a slope of 2 confirms that it is a two-photon excited upconverted PL. When the excitation power increases further, the PL intensity tends to be saturated as shown in Fig. 2(c). This phenomenon matches with the MPAPS method, which provides a simple and effective method to evaluate the MPA cross-section of NCs.^[27] Considering the rapid Auger recombination in perovskite NCs, it can be known that multiple exciton species do not contribute to PL. Therefore, no matter how many photons are absorbed by the NCs, only one photon can be emitted. The integrated PL intensity is given by the following formula:^[27]

$$I_{\text{PL}} = \gamma\eta(1 - P(0)), \quad (1)$$

where I_{PL} is the integrated PL intensity, η is the quantum yield of the FAPbBr₃ NCs, γ is the collection/detection efficiency, and $P(0)$ is the probability that an NC does not produce excitons. Considering that the process of absorbing photons in

NCs conforms to the Poisson distribution, the probability of generating i excitons in an NC is^[28]

$$P(i) = \frac{\langle N \rangle^i e^{-\langle N \rangle}}{i!}, \quad i = 0, 1, 2, \dots, \quad (2)$$

where $\langle N \rangle$ is the average number of excitons per NC. Thus, equation (1) can be modified to

$$I_{\text{PL}} = \gamma\eta \left(1 - e^{-\langle N \rangle}\right). \quad (3)$$

In general, for TPA process, the effective absorption coefficient is given by^[29]

$$\alpha = \alpha_1 + \alpha_2 \times I, \quad (4)$$

where I is the excitation intensity, α_1 and α_2 are the linear absorption and TPA coefficients, respectively. Therefore, the TPA cross-section σ_2 is^[30]

$$\sigma_2 = (\hbar\omega) \frac{\alpha_2}{N_A \times C_{\text{NC}} \times 10^{-3}}, \quad (5)$$

where $\hbar\omega$ is the photon energy, N_A is Avogadro constant, C_{NC} is the NCs concentration in the sample, which is determined to be 64.636 ppb here via ICP-MS. Considering that the excitation pulse possesses a Gaussian profile, the photon flux $\langle \Phi \rangle$ and $\langle N \rangle$ can be defined as

$$\langle \Phi \rangle = \frac{2P}{(\pi r^2)(\hbar\omega)}, \quad (6)$$

$$\langle N \rangle = \frac{\sigma_2 \langle \Phi \rangle^2}{2\sqrt{2} T \sqrt{\pi}}, \quad (7)$$

where P is the excitation power, and r is the beam spot radius. The corresponding TPA cross-section is

$$\sigma_2 = \left(2\sqrt{2}\pi\right) \langle N \rangle \frac{T}{\langle \Phi \rangle^2}. \quad (8)$$

As shown in Fig. 2(c), plotting PL intensity as a function of $\langle \Phi \rangle^2/T$, and fitting by Eq. (8), the TPA cross-section of $2.76 \times 10^{-45} \text{ cm}^4 \cdot \text{s} \cdot \text{photon}^{-1}$ can be obtained. The main issues which introduce experimental errors are the spot size, pulse width, and excitation power. The value of $\langle N \rangle$ obtained from the fittings also has fitting error. However, it is typically much smaller than the other errors and can be neglected. Consequently, the estimated error of $\Delta\sigma_2$ is

$$\frac{\Delta\sigma_2}{\sigma_2} = \sqrt{\left(\frac{\Delta T}{T}\right)^2 + \left(\frac{2\Delta P}{P}\right)^2 + \left(\frac{4\Delta r}{r}\right)^2}. \quad (9)$$

For our experiments, the errors of the spot size, pulse width, and excitation power is 0.02, 0.03, and 0.03, respectively. Based on the estimation, the experimental error of TPA cross-section is about 3.8%.

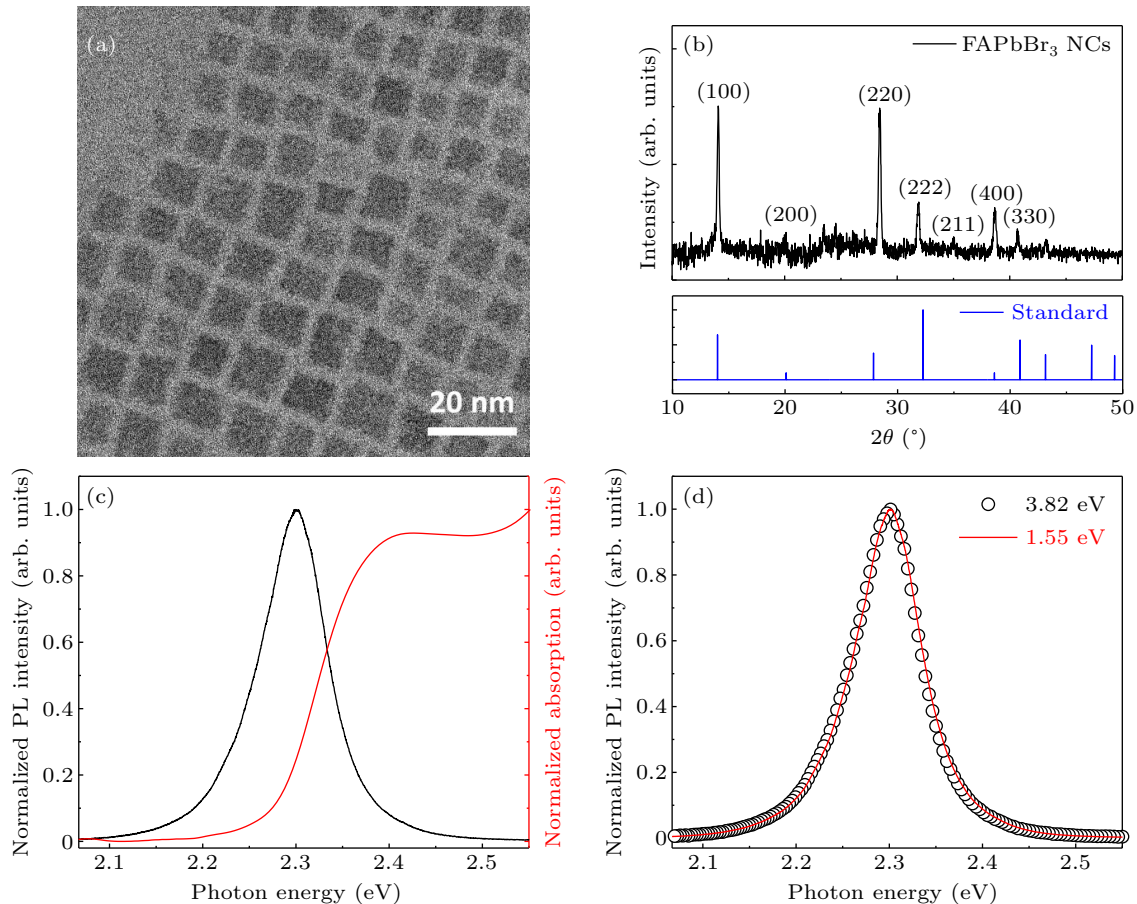


Fig. 1. Characterization of FAPbBr₃ NCs: (a) TEM image, (b) XRD patterns, (c) absorption and PL spectra, (d) one- and two-photon excited PL spectra.

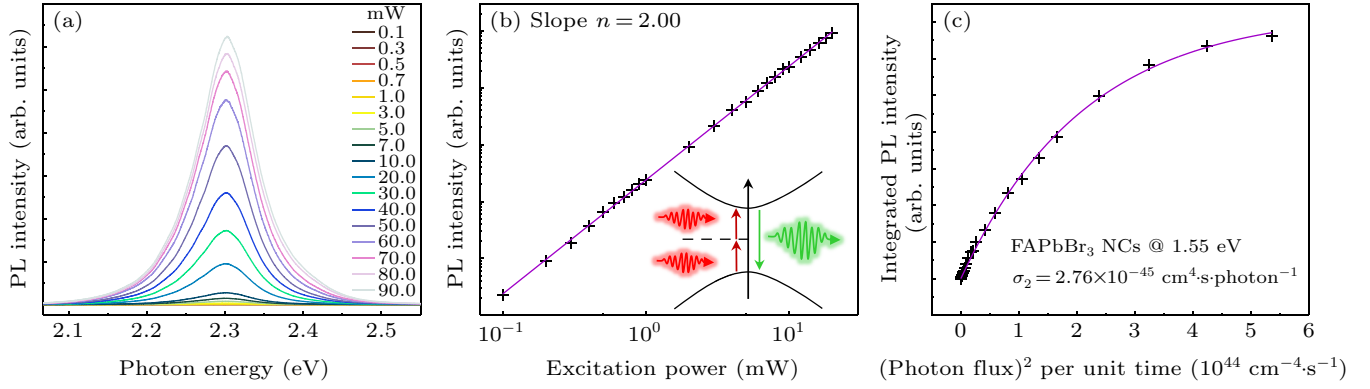


Fig. 2. (a) Power-dependent PL spectra from 0.1 mW to 90 mW, (b) the quadratic dependence on the excitation power of the PL intensity. Inset shows the two-photon PL emission process. (c) MPAPS fitting curve at 800 nm.

Table 1. Summary of TPA cross-section of perovskite nanocrystals.

Perovskite materials	TPA cross-section ($10^{-50} \text{ cm}^4 \cdot \text{s-photon}^{-1}$)	Excitation wavelength (nm)	Pulse width, repetition rate	Size (nm)
CsPbCl ₃ ^[31,32]	3.8×10^4	700	100 fs, 80 MHz	5
CsPbCl ₃ :Mn ^[33]	7.0×10^3	620	100 fs, 1 kHz	9.8
CsPbCl _{1.5} Br _{1.5} ^[31]	8.7×10^4	620	– fs, 1 kHz	7.8
CsPbBr ₃ ^[31]	8.8×10^4	800	100 fs, 80 MHz	5–7
CsPbBr ₃ ^[31]	1.8×10^5	800	100 fs, 80 MHz	6
Cs ₄ PbBr ₆ ^[34]	2.3×10^7	800	70 fs, 1 kHz	20
CsPb _{0.8} Zn _{0.2} I ₃ ^[35]	$(1.5 - 3.8) \times 10^5$	740–880	100 fs, 1 kHz	12.7
CsPbI ₃ ^[31,36]	2.1×10^6	1500	100 fs, 80 MHz	7
MAPbBr ₃ ^[17,37]	2.1×10^4	925	– fs, 1 kHz	17
MAPbBr ₃ ^[17,37]	5.2×10^6	800	130 fs, 76 kHz	5
MAPbBr ₃ /(OA) ₂ PbBr ₄ ^[17]	8.0×10^5	800	50 fs, 1 kHz	8–9
MAPbBr ₃ /(OA) ₂ PbBr ₄ ^[17]	$(3.3 - 40.2) \times 10^6$	675–1000	50 fs, 1 kHz	9–10
FAPbBr ₃	2.76×10^5	800	100 fs, 1 kHz	10

Meanwhile, the Z-scan technique was carried out to double check the accuracy of the obtained TPA cross-section. It is noted that the n-hexane solution reveals no NLO signal, even under the maximum excitation density ($382.2 \text{ GW} \cdot \text{cm}^{-2}$) used herein, which ensures the observed NLO behavior mainly originates from the FAPbBr₃ NCs. In Fig. 3(b), with the increase of excitation intensity, the NCs exhibits simple-valley-structured curves (the reverse saturable absorption), which is a typical feature of TPA. The experimental data can be fitted by applying a well-established formula as follows:^[29]

$$T(z) = \sum_{m=0}^{\infty} \frac{\left(\frac{-\alpha_0 L_{\text{eff}}}{1+z^2/z_0^2} \right)^m}{m+1}, \quad (10)$$

where $L_{\text{eff}} = (1 - e^{-\alpha_1 L}) / \alpha_1$ represents the effective interaction length, L is the sample thickness, z is the longitudinal displacement of the sample from the focus ($z = 0$), and z_0 is the Rayleigh diffraction length. The TPA coefficient is obtained up to around 0.00085 cm/GW . By the virtue of Eq. (5), the TPA cross-section calculated by Z-scan technique is $2.67 \times 10^{-45} \text{ cm}^4 \cdot \text{s-photon}^{-1}$, which is close to the value obtained above. In order to better understand the NLO properties of FAPbBr₃ NCs, the TPA cross-section is compared with other perovskite materials and listed in Table 1. Because

the TPA cross-section is closely related to the volume of NCs, and the NLO properties of the same materials under different excitation conditions (wavelength, pulse width, and repetition rate) are also very different, the data in the table can only be used as a reference. Nevertheless, the TPA cross-section of FAPbBr₃ NCs is nearly the smallest, which implies that FAPbBr₃ can achieve strong nonlinear absorption behavior.

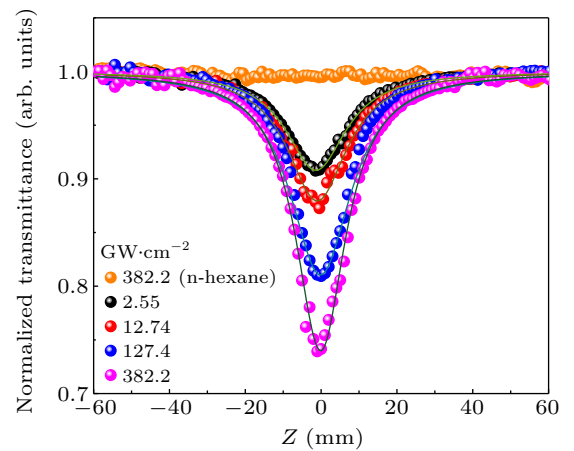


Fig. 3. OA Z-scan results for FAPbBr₃ NCs under different excitation intensities.

Obviously, the TPA cross-section of FAPbBr₃ NCs obtained is much smaller than that of other

perovskites.^[15,17,38–40] It is necessary to clarify the reason. It is well known that the TPA cross-section is closely related to the NLO properties, which in turn originates from the distortion of electron cloud. The NLO properties of perovskites are determined by the conduction band (CB),^[41] which is contributed by the p orbit of Pb^{2+} . According to our previous report, it is realized that the large size of FA^+ cation and the strong interaction of hydrogen bonds directly will lead to the increase of Pb–I bond length and Pb–I–Pb bond angle, weakening the traction of I^- to Pb^{2+} and reducing Pb^{2+} electron cloud distortion.^[23] In addition, the dipoles in FAPbBr_3 NCs are almost impossible to show any rotational dynamics at room temperature, that is, they are in a deep-frozen glassy state, which results in an extremely small TPA cross-section.^[42]

The measurement of temperature dependent PL induced by TPA from 80 K to 295 K was carried out to analyze the NLO behavior in FAPbBr_3 NCs, and the results are depicted in Fig. 4(a). In Fig. 4(b), the power-law dependence of the inte-

grated PL intensity with the excitation power is 1.979 at 80 K, which suggests the TPA process and the excitonic recombination. The integrated PL intensity, FWHM, and emission photon energy of FAPbBr_3 NCs with temperature are summarized in Fig. 4(c). Due to the structural phase transition, the photon energy remains almost constant below 140 K (green line). Then, with the increase of temperature from 140 K to 295 K, it exhibits a blueshift, which can be attributed to the stability of the out-of-phase band edge state with the lattice expansion. The photon energy can be fitted well by^[43]

$$E = E_0 - \frac{aT^2}{T+b}, \quad (11)$$

where E_0 is the is the unrenormalized bandgap at 0 K, a is the temperature coefficient of FAPbBr_3 NCs, and b is the parameter related to the Debye temperature. The fitted a of $0.360 \text{ meV}\cdot\text{K}^{-1}$ is similar to those reported data in other literatures,^[20,44,45] implying the colloidal FAPbBr_3 NCs has great advantages in temperature sensors with high sensitivity.

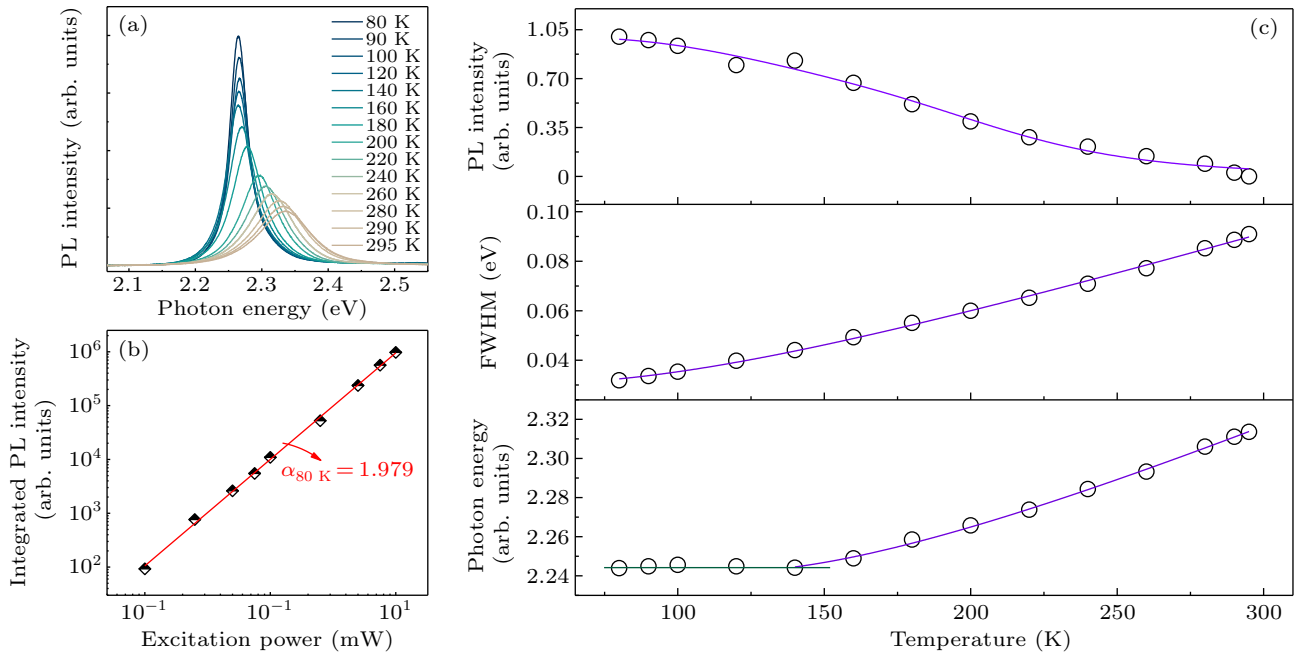


Fig. 4. (a) Temperature-dependent PL spectra of FAPbBr_3 NCs. (b) The variation of integrated PL intensity with excitation power for FAPbBr_3 NCs at 80 K and 295 K. (c) Photon energy, FWHM, and integrated PL intensity as a function of temperature extracted from panel (a).

Under constant pressure, the temperature dependence of the bandgap is generally estimated by the following expression under a quasi-harmonic approximation:^[46]

$$\frac{\partial E_g}{\partial T} = \frac{\partial E_g}{\partial V} \frac{\partial V}{\partial T} + \sum_{j,q} \left(\frac{\partial E_g}{\partial n_{j,q}} \right) \left(n_{j,q} + \frac{1}{2} \right), \quad (12)$$

where $n_{j,q}$ is the number of phonons at j branch with wave vector of q . The first part of Eq. (12) describes the contribution of the thermal expansion of the lattice, while the second part is attributed to the EP interaction. Obviously, the large value of the temperature coefficient in FAPbBr_3 NCs may caused by the strong lattice expansion, which is consistent with the large

size of FA^+ cation. Meanwhile, the weak EP coupling should be another plausible origin.

In order to discuss the EP coupling mechanism in FAPbBr_3 NCs, temperature-dependent emission broadening was explored. The emission bandwidth can be expressed as^[46]

$$\Gamma(T) = \Gamma_0 + \gamma_{\text{LO}} \frac{1}{\exp(E_{\text{LO}}/k_{\text{B}}T)}, \quad (13)$$

where k_{B} is the Boltzmann constant, Γ_0 is the term of a temperature-independent inhomogeneous broadening, which results from the disorder and imperfection scattering. The second term is the homogeneous broadening, which arises

from LO phonon–carrier scattering. γ_{LO} and E_{LO} are EP coupling strength and the LO phonon energy, respectively. From the PL spectra, these parameters are derived to be $E_{LO} = 16.900$ meV and $\gamma_{LO} = 44.464$ meV. Compared with CsPbBr₃ and MAPbBr₃, the cationic charge value in FAPbBr₃ NCs is only $0.65e$,^[47] resulting in the smallest LO phonon energy, which means the most weak oscillation of the ionic Pb–Br sub-lattice. This conclusion is consistent with our previous report that a larger cation size and strong hydrogen bonds interaction greatly weaken the traction of Br[−] to Pb²⁺.^[23] Naturally, FAPbBr₃ NCs display weaker NLO response. Moreover, the EP coupling strength is related to polarons.^[48] It has been claimed that the formation, dynamics, and recombination of polarons arise principally from the modulation of inorganic framework [PbBr₆]^{4−} rather than the dipole nature of A cations.^[49] The above two factors also cause serious distortion of the inorganic framework in FAPbBr₃, which directly lead to the large polaron protection shield formed around an electron or a hole. In this case, the Coulomb interaction responsible for LO phonon scattering is screened.^[48] This is why the EP coupling strength (γ_{LO}) of FAPbBr₃ NCs is smaller than other perovskites. Generally speaking, the small polaron make significant contribution to the nonlinear absorption.^[50] In contrast, the large polarons in FAPbBr₃ will reduce the NLO response significantly.

Furthermore, the integrated PL intensity decreases with the increase of temperature from 80 K to 295 K. With the increase of temperature, the PL quenching can be ascribed to the thermal activation of nonradiative recombination centers and the enhanced EP coupling. The corresponding integrated PL intensity can be fitted by the following equation:^[46]

$$I(T) = \frac{I_0}{1 + CT \exp(-E_1/k_B T)}, \quad (14)$$

where I_0 is the PL intensity at 0 K, C is constant, E_1 is the exciton binding energy, which is determined to be approximately 69.668 meV. This value is well consistent with the reported literatures.^[37,51,52] It is realized that the exciton binding energy of FAPbBr₃ NCs is larger than that of other perovskites like CsPbBr₃ and MAPbBr₃ NCs,^[51,53,54] which may caused by the strong interaction of hydrogen bonds.

Finally, the long-term stability of perovskite NCs is of paramount importance for their application in optoelectronic devices. Hence, the relevant experiment under 300 K and 40% relatively humidity was conducted, and the sample was illuminated continuously upon 800-nm excitation with the power of 10.0 mW. As shown in Fig. 5, it can be seen that the PL intensity maintains about 70.5% of the initial intensity after 600 minutes. The inset shows the time dependent PL spectrum of the FAPbBr₃ NCs. There is still a way to go for the practical applications, and methods needs to be used to further

strengthen the long-term stability, such as the construction of core–shell structure, ion doping, *etc.*^[55–58]

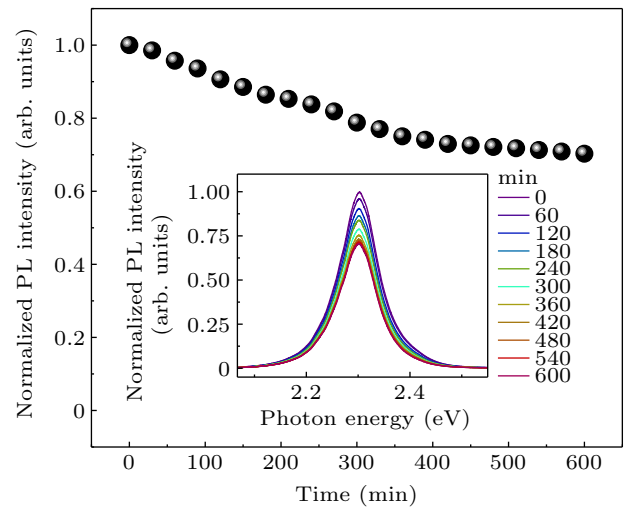


Fig. 5. Photostability of FAPbBr₃ NCs under 800 nm. Inset: time-dependent PL spectra.

4. Conclusion

In summary, the TPA cross-section of FAPbBr₃ NCs at 800 nm was determined to be 2.76×10^{-45} cm⁴·s·photon^{−1} by using MPAPS, and was corroborated by OA Z-scan technique. The obtained value is much smaller than that of other perovskites, which can be ascribed to the large size of FA⁺ cation, strong interaction of hydrogen bonds, as well as the dipoles in deep-frozen glassy state. Moreover, the emission characteristics induced by TPA was investigated by temperature-dependent PL spectroscopy. The small LO-phonon energy and EP coupling strength caused by the serious distortion of the inorganic framework [PbBr₆]^{4−} confirmed the weaker NLO response. The exciton binding energy of 69.668 meV in FAPbBr₃ NCs was obtained, explaining the strong hydrogen bonding effect. The extremely small TPA cross-section in FAPbBr₃ NCs can achieve strong nonlinear absorption behavior, which is useful for low-cost nonlinear absorbers and high-performance optoelectronic devices, as well as light collection applications.

Acknowledgments

Project supported by the National Natural Science Foundation of China (Grant No. 62174079) and the Fund from the Science, Technology, and Innovation Commission of Shenzhen Municipality (Grant Nos. JCYJ20220530113015035, JCYJ20210324120204011, JCYJ20190808121211510, and KQTD2015071710313656).

References

- [1] Sumalekshmy S and Fahrni C J 2011 *Chem. Mater.* **23** 483
- [2] Dahlstedt E, Collins H A, Balaz M, Kuimov M K, Khurana M, Wilson B C, Phillips D and Anderson H L 2009 *Org. Biomol. Chem.* **7** 897

- [3] Heinemann F, Karges J and Gasser G 2017 *Acc. Chem. Res.* **50** 2727
- [4] Sánchez E J, Novotny L, Holtom G R and Xie X S 1997 *J. Phys. Chem. A* **101** 7019
- [5] Mohanty S K, Reinscheid R K, Liu X, Okamura N, Krasieva T B and Berns W B 2008 *Biophys. J.* **95** 3916
- [6] Bethge P, Chéreau R, Avignone E, Marsicano G and Nägerl U V 2013 *Biophys. J.* **104** 778
- [7] He G S, Xu G C, Prasad P N, Reinhardt B A, Bhatt J C and Dillard A G 1995 *Opt. Lett.* **20** 435
- [8] Chong E, Watson T and Festy F 2014 *Appl. Phys. Lett.* **105** 062111
- [9] Cumpston B H, Ananthavel P S, Barlow S, Dyer D L, Ehrlich J E, Erskine L L, Heikal A A, Kuebler S M, Lee I Y S, McCord-Maughon D, Qin J, Röckel H, Rumi M, Wu X L, Marder S R and Perry J W 1999 *Nature* **398** 51
- [10] Yong K T, Qian J, Roy I, Lee H H, Bergey E J, Trampusch K M, He S, Swihart M T, Maitra A and Prasad P N 2007 *Nano Lett.* **7** 761
- [11] Albota M, Beljonne D, Brédas J L, Ehrlich J E, Fu J Y, Heikal A A, Hess S E, Kogej T, Levin M D, Marder S R, Mccord-Maughon D, Perry J W, Röckel H, Rumi M, Subramaniam G, Webb W W, Wu X L and Xu C 1998 *Science* **281** 1653
- [12] Albota M A, Xu C and Webb W W 1998 *Appl. Opt.* **3** 735
- [13] Zhu B, Zhang H C, Zhang Z Y, Cui Y P and Zhang J Y 2011 *Appl. Phys. Lett.* **99** 021908
- [14] Zhu B H, Zhang H C, Zhang Z Y, Cui Y P and Zhang J Y 2011 *Appl. Phys. Lett.* **99** 231903
- [15] Chen J, Židek K, Chábera P, Liu D, Cheng P, Nuuttila L, Al-Marri M J, Lehtivuori H, Messing M E, Han K, Zheng K and Pullerits T 2017 *J. Phys. Chem. Lett.* **8** 2316
- [16] Walters G, Sutherland B R, Hoogland S, Shi D, Comin R, Sellan D P, Bakr O M and Sargent E H 2015 *ACS Nano* **9** 9340
- [17] Chen W, Bhaumik S, Veldhuis S A, Xing G, Xu Q, Grätzel M, Mhaisalkar S, Mathews N and Sum T C 2017 *Nat. Commun.* **8** 15198
- [18] Zareba J K, Nyk M and Samoć M 2021 *Adv. Opt. Mater.* **9** 2100216
- [19] Liu Z, Hu P, Zhang Z, Du J, Yang J, Tang X, Liu W and Leng Y 2019 *ACS Photon.* **6** 3150
- [20] Yang L, Wei K, Xu Z, Li F, Chen R, Zheng X, Cheng X and Jiang T 2018 *Opt. Lett.* **43** 122
- [21] Minh D N, Kim J, Hyon J, Sim J H, Sowlih H H, Seo C, Nam J, Eom S, Suk S, Lee S, Kim E and Kang Y 2017 *Chem. Mater.* **29** 5713
- [22] Zhang F, Yang B, Zheng K, Yang S, Li Y, Deng W and He R 2018 *Nano-Micro Lett.* **10** 43
- [23] Zhang X, Xiao S, Li R, He T and Chen R 2020 *Photon. Res.* **8** A25
- [24] Zu Y, Xi J, Li L, Dai J, Wang S, Yun F, Jiao B, Dong H, Hou X and Wu Z 2019 *ACS Appl. Mater. Interfaces* **12** 2835
- [25] Protesescu L, Yakunin S, Bodnarchuk M I, Bertolotti F, Masciocchi N, Guagliardi A and Kovalenko M V 2016 *J. Am. Chem. Soc.* **138** 14202
- [26] Wang J, Song C, He Z, Mai C, Xie G, Mu L, Cun Y, Li J, Wang J, Peng J and Cao Y 2018 *Adv. Mater.* **30** 1804137
- [27] Alo A A, Barros L W T, Nagamine G, Vicira L B, Chang J H, Jeong B G, Bae W K and Padilha L A 2020 *ACS Photon.* **7** 1806
- [28] Klimov V I 2007 *Annu. Rev. Phys. Chem.* **58** 635
- [29] Sheik-Bahae M, Said A A, Wer T H, Hagan D J and Van Stryland E W 1990 *IEEE J. Quantum Electron.* **26** 760
- [30] Li X, Embden J, Chon J W M and Gu M 2009 *Appl. Phys. Lett.* **94** 103117
- [31] Pramanik A, Gates K, Gao Y, Begum S and Ray P C 2019 *J. Phys. Chem. C* **123** 5150
- [32] Li J, Ren C, Qiu X, Lin X, Chen R, Yin C and He T 2018 *Photon. Res.* **6** 554
- [33] He T, Li J, Qiu X, Xiao S and Lin X 2018 *Photon. Res.* **6** 1021
- [34] Krishnakanth K N, Seth S, Samanta A and Rao S V 2019 *Nanoscale* **11** 945
- [35] Zhao F, Li J, Yu J, Guo Z, Xiao S, Gao Y, Pan R, He T and Chen R 2020 *J. Phys. Chem. C* **124** 27169
- [36] Szeremeta J, Antoniak M A, Wawrzyńczyk D, Nyk M and Samoć M 2020 *Nanomaterials* **10** 1054
- [37] Lu W G, Chen C, Han D, Yao L, Han J, Zhong H and Wang Y 2016 *Adv. Opt. Mater.* **4** 1732
- [38] Zhang W, Peng L, Liu J, Tang A, Hu J S, Yao J and Zhao Y S 2016 *Adv. Mater.* **28** 4040
- [39] Krishnakanth K N, Seth S, Samanta A and Rao S V 2019 *Nanoscale* **11** 945
- [40] Li J, Zhao F, Xiao S, Cheng J, Qiu X, Lin X, Chen R and He T 2019 *Opt. Lett.* **44** 3873
- [41] Liu Y Q, Cui H L and Wei D 2018 *J. Phys. Chem. C* **122** 4150
- [42] Govinda S, Kore B P, Swain D, Hossain A, De C, Row T N G and Sarma D D 2018 *J. Phys. Chem. C* **122** 13758
- [43] Varshni Y P 1967 *Physica* **34** 149
- [44] Wang X, Wang Q, Chai Z and Wu W 2020 *RSC Adv.* **10** 44373
- [45] Dai J, Zheng H, Zhu C, Lu J and Xu C 2016 *J. Mater. Chem. C* **4** 4408
- [46] Zhang X Y, Pang G T, Xing G C and Chen R 2020 *Mater. Today Phys.* **15** 100259
- [47] Lindblad R, Jena N K, Philippe B, Oscarsson J, Bi D, Lindblad A, Mandal S, Pal B, Sarma D D, Karis O, Siegbahn H, Johansson E M J, Odelius M and Rensmo H 2015 *J. Phys. Chem. C* **119** 1818
- [48] Zhu H, Miyata K, Fu Y, Wang J, Joshi P P, Niesner D, Williams K W, Jin S and Zhu X Y 2016 *Science* **353** 1409
- [49] Munson K T, Swartfager J R, Gan J and Asbury J B 2020 *J. Phys. Chem. Lett.* **11** 3166
- [50] Badorreck H, Nolte S, Freytag F, Bäune P, Dieckmann V and Imlau M 2015 *Opt. Mater. Express* **5** 2729
- [51] Galkowski K, Mitioglu A, Miyata A, Plochocka P, Portugall O, Eperon G E, Wang J T W, Stergiopoulos T, Stranks S D, Snaith H J and Nicholas R J 2016 *Energy Environ. Sci.* **9** 962
- [52] Han D, Imran M, Zhang M, Chang S, Wu X G, Zhang X, Tang J, Wang M, Ali S, Li X, Yu G, Han J, Wang L, Zou B and Zhong H 2018 *ACS Nano* **12** 8808
- [53] Sestu N, Cadelano M, Sarritzu V, Chen F, Marongiu D, Piras R, Mainas M, Quochi F, Saba M, Mura A and Bongiovanni G 2015 *J. Phys. Chem. Lett.* **6** 4566
- [54] Shulenberg K E, Ashner M N, Ha S K, Krieg F, Kovalenko M V, Tisdale W A and Bawendi M G 2019 *J. Phys. Chem. Lett.* **10** 5680
- [55] Zhang X, Guo Z, Li R, Yu J, Yuan B, Chen B, He T and Chen R 2021 *ACS Appl. Mater. Interfaces* **13** 58170
- [56] Jia C, Li H, Meng X and Li H 2018 *Chem. Commun.* **53** 6300
- [57] Dong Y, Yan D, Yang S, Wei N, Zou Y and Zeng H 2023 *Chin. Phys. B* **32** 018507
- [58] Ma W, Ding C, Wazir N, Wang X, Kong S, Li A, Zou B and Liu R 2022 *Chin. Phys. B* **31** 037802